DISCRIMINATION OF SEA ICE EDGE IN THE ANTARCTIC, FROM NOAA MSU

Takashi YAMANOUCHI

National Institute of Polar Research, 9-10, Kaga 1-chome, Itabashi-ku, Tokyo 173

and

Yoichi SEO

University of Electro-Communications, 5-1, Chofugaoka 1-chome, Chofu-shi, Tokyo 182

Abstract: Discrimination of the sea ice edge is done using the microwave 50.3 GHz brightness temperature measured by NOAA satellites. Considering the emissivity variation between the open sea and sea ice, the contour of 232 K brightness temperature is regarded as the ice edge. The method is very simple but contains several sources of uncertainty owing to the atmospheric effect and low resolution. Limits and possibilities of the method are discussed. Horizontal distributions of sea ice are compared to the AVHRR imagery and good agreement is found. An annual variation of sea ice distribution is presented.

1. Introduction

Knowing the variation of the sea ice edge in the polar region is urgent not only for the study of local heat exchange between the sea and atmosphere, but also for the study of global climate. Since surface measurements are scarce, great reliance is placed on satellite remote measurements. Satellite observations of sea ice distribution have been made using visible and infrared imagery; however, we cannot use visible images in the polar night and clouds obscure the surface image in the visible and infrared. Microwave observations have the defect of low resolution on account of the antenna geometry; however, they are powerful in searching a large-scale sea ice distribution irrespective of day and night and also are not affected seriously by clouds. Passive microwave observations detect the difference in surface emissivity. Sea ice detection, is facilitated by the large difference in surface emissivity between open sea and sea ice, which produces high contrast.

Studies of passive microwave remote sensing from satellites started in the 1960's. From the measurement of Arctic sea ice by airborne microwave radiometer, WILHEIT *et al.* (1972) found that there is a large difference in microwave emissivity between open sea and sea ice, and that there is also some difference in emissivity between the first-year ice and multi-year ice. Owing to these, the 19 GHz Electric Scanning Microwave Radiometer (ESMR) on Nimbus-5 provided many monthly distributions of sea ice in the Southern Ocean from 1973 to 1976 (ZWALLY *et al.*, 1983). More recently, Scanning Multichannel Microwave Radiometer (SMMR) on Nimbus-7 was

used to distinguish different ice types—first-year, multi-year, etc. (COMISO, 1983). However, the emissivity of sea ice, the sea ice concentration derived from microwave emissivity and the definition of sea ice edge have not been adequately established yet, and extensive studies of ground truth (sea truth) are yet to be made (COMISO and ZWALLY, 1982; COMISO *et al.*, 1984).

In the present study, using the 50.3 GHz data of the Microwave Sounding Unit (MSU) aboard TIROS-N/NOAA series meteorological satellites, we tried to derive the sea ice edge in the Southern Ocean. Since the primary objective of the MSU was to retrieve the atmospheric temperature profile from the absorption of the oxygen 0.5 cm band, rather than to sense the surface parameters, it is difficult to obtain surface information in spite of using the 50.3 GHz "window channel". However, these satellites are operational and the data are received at Syowa Station (69°00'S, 39°35'E) every day, and results have a potential to be analyzed in real time.

2. MSU Data and Analytical Method

Radiometers of MSU aboard TIROS-N/NOAA series satellites aim to obtain the vertical temperature distribution by measuring thermal emission in the oxygen 0.5 cm band. The MSU consists of four Dicke-type radiometers with antenna beam widths 7.5°, and a cross-track scan yields foot prints as shown in Fig. 1. The field of view at nadir is about 110 km in diameter, but more than 300 km in length at the edge of the scan. Each radiometer is calibrated against a monitored target in the satellite and 2.7 K cold space temperature. Fluctuations in the brightness temperature measurements are reported as 0.25 K by SMITH *et al.* (1979) and by GRODY and SHEN (1982).

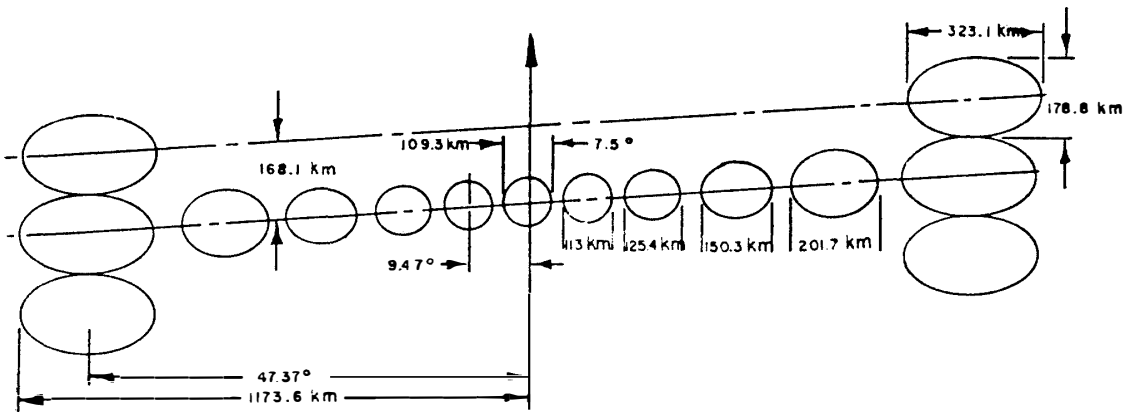

Fig. 1. MSU scan grid pattern and field of view (half-power) projected on Earth. The orbit is circular with a radius of 833 km (GRODY and SHEN, 1982).

Four MSU channels have their center frequencies at 57.95, 54.96, 53.73 and 50.31 GHz, respectively. From the difference of absorptivity, their weighting functions peak at 90, 300, 700 mb and the ground surface, respectively. The transmittance for the standard atmosphere is shown in Fig. 2 and weighting functions are in Fig. 3. In the present analysis, we use the 50.3 GHz window channel (channel 1) which contains

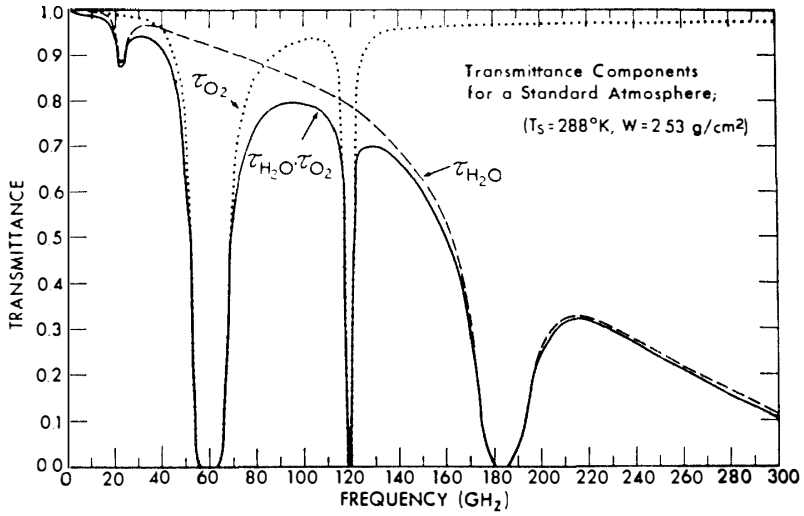

Fig. 2. Transmittances in microwave region calculated for path between the surface and space for O_2, H_2O and their product (WEINREB et al., 1981).

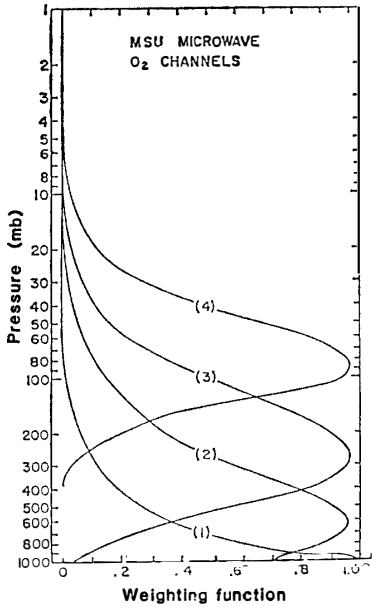

Fig. 3. Weighting functions of four channels of the MSU, normalized at peak value. Channel 1 (50.31 GHz), 2 (53.73), 3 (54.96) and 4 (57.95) (SMITH et al., 1979).

more information on the surface than other channels. Though the channel 1 is in the window region, it still has some weights in the atmosphere as seen in Figs. 2 and 3, so special care should be taken in obtaining the surface information.

The brightness temperature T_B of the microwave radiance measured by radiometers is expressed as,

$$T_B = \varepsilon T_s \tau + (1-\varepsilon) T_A \tau - \int_0^{p_S} T(p) \frac{\partial \tau}{\partial p} \mathrm{d}p, \qquad (1)$$

where ε is the surface emissivity, T_S is the surface temperature, τ is the transmittance of the atmosphere, T_A is the brightness temperature of the atmosphere and sky

measured at the surface, $T(p)$ is the temperature at the level of pressure p and p_S is the surface pressure. T_A can be written as,

$$T_A = T_{\text{Space}} \cdot \tau + \int_0^{p_S} T(p) \frac{\partial \tau(p_S - p)}{\partial p} \, dp. \qquad (2)$$

The first term in eq. (1) is the surface emission, the second term is the reflected radiation of the atmosphere and sky radiation and the third term is the atmospheric component emitted upwards. To obtain information on the surface, it is appropriate to chose the wavelength region where the atmospheric effect is negligible—the second and thrid terms of eq. (1) are negligible and τ is close to 1. However, in the present data at 50.3 GHz, effects of the second and third terms of eq. (1) and τ cannot be neglected.

Table 1. Atmospheric effects of MSU 50.3 GHz channel.

	τ	T_A	Third term of eq. (1)
Summer (October–March)	0.713	73.4 K	70.6 K
Winter (April–September)	0.704	73.7 K	71.1 K
Annual mean	0.709	73.5 K	70.9 K

The transmittance from the space to the surface, τ, T_A and the third term of eq. (1) are calculated (Table 1). Calculations are made using the method by WEINREB *et al.* (1981) for the mean temperature and humidity profiles at Syowa Station (JAPAN METEOROLOGICAL AGENCY, 1982) under clear sky. Using these annual mean values, eq. (1) is rewritten as,

$$T_B = 123 + 0.709\varepsilon \, (T_S - 73.5). \qquad (3)$$

If we assume the surface temperature to be at the freezing point of sea water, $-2°C$, then T_B is approximated as,

$$T_B = 123 + 140\varepsilon. \qquad (4)$$

The difference in ε can be uniquely expressed by the difference in T_B.

The open sea and sea ice can be distinguished by the difference of T_B, since a large difference in ε at the surface exists. The emissivity of the open sea is about 0.5 and that of the first-year sea ice is about 0.9 (WILHEIT *et al.*, 1972; WILHEIT, 1978; SVENDSEN *et al.*, 1983). From eq. (3) variations of T_B owing to the variation of T_S or ε are estimated as,

$$\delta T_B / \delta T_S = 0.709\varepsilon \approx 0.5,$$
$$\delta T_B / \delta \varepsilon = 0.709 \, (T_S - 73.5) \approx 140.$$

If the surface varied from the open sea to the sea ice, $\delta\varepsilon \approx 0.4$ and $\delta T_B \approx 56$ by assuming no change in the surface temperature at 271 K. On the other hand, the variation of T_S of the sea ice near the ice edge is within about 20 K from the estimate

by MAYKUT (1978) in most of the season. Then δT_B becomes 10K. It is possible to detect the sea ice. It would become more precise to estimate these errors if the surface temperature was actually obtained from the satellite data concurrently.

The sea surface condition and clouds are liable to be sources of errors in detecting the sea ice. Foam caused by wind blowing on the surface will affect the emissivity (NORDBERG *et al.*, 1971; WILHEIT, 1978). From the results at 19.35 GHz, the brightness temperature of the sea surface will be increased at a rate of $1\,K/ms^{-1}$ by wind stronger than 7 m/s. Since this is the effect at the surface, T_B will be increased about 10K by a 20 m/s wind. The effect of clouds will appear in the transmission function due to the extinction of cloud particles. The increase of T_B by clouds was calculated by GRODY and SHEN (1982) as shown in Fig. 4. Since we have no information about the liquid water content of clouds in the Antarctic region, some climatological mean values are derived from STEPHENS (1978). He reported that the density of the stratus was about $0.2\,g/m^3$ in average and about $0.5\,g/m^3$ at the maximum. If we assume the cloud thickness to be 1 km, the total liquid water content will be about 0.02 to $0.05\,g/m^2$, resulting in a 5–10K increase in T_B for a nonprecipitating cloud (see Fig. 4).

Several factors responsible for errors in measuring the surface information are

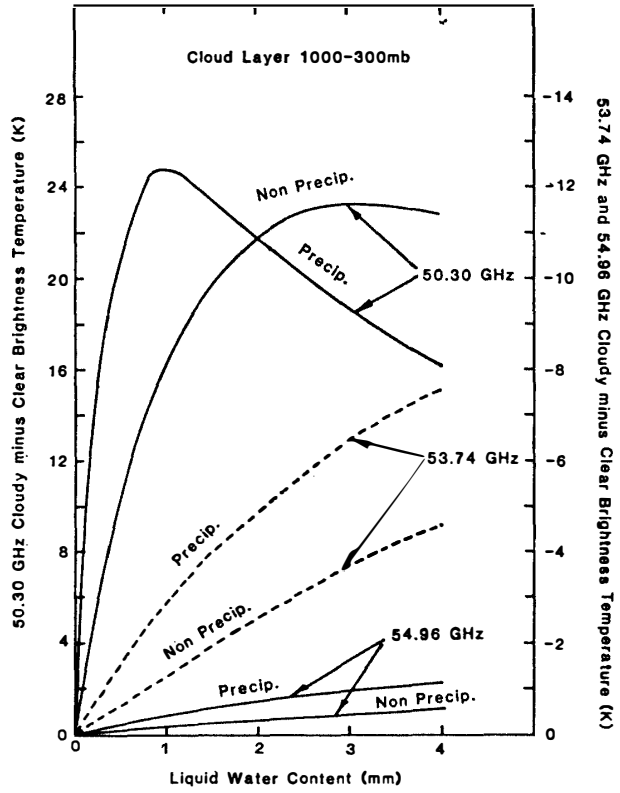

Fig. 4. Simulated liquid water effects on MSU channels. Cloudy minus clear brightness temperature values are plotted against liquid water content. Results are shown separately for large drops (precipitating) and small drops (non precipitating) which are distributed from the sea surface to the 300-mb level (GRODY and SHEN, 1982).

examined, and about 20 K uncertainty is expected for the brightness temperature T_B measured from space. This uncertainty will amount to an error of 30% for an emissivity variation from 0.5 to 0.9. It is difficult to deduce the concentration or to classify the age of sea ice, except for the restricted conditions of clear sky, calm wind and small surface temperature difference. The difference in emissivity according to type of sea ice is larger in the 50 GHz region than in the 10 GHz region (WILHEIT *et al.*, 1972); however, seen from space, the atmospheric effect makes it difficult to classify sea ice. The low resolution of the MSU also creates difficulties.

3. Distribution of Sea Ice

A total of 120 orbital data of NOAA-6 and -7 are analyzed among the data from 700 orbits received at Syowa Station by the second author (Y. SEO) during the 22nd Japanese Antarctic Research Expedition in 1981 to 82 (JARE-22). The foregoing data processing, derivation of CCT from high density data (HRPT), and retrieval of MSU data from TOVS (TIROS Operational Vertical Sounder), was performed by the method already reported elsewhere (TANAKA *et al.*, 1982). Data of channel 1, 50.3 GHz, of the MSU were used in the analysis after the calibration and limb correction were done.

An example of 50.3 GHz brightness temperature along the nadir points—approximately parallel to the meridian—is shown in Fig. 5. From lower latitudes to 62°S the brightness temperature is constant, about 212–213 K, which corresponds to the open sea (this region appears almost clear on AVHRR infrared images). The brightness temperature increases greatly from 62.1°S, and is 241 K at 63.6°S. Most of the

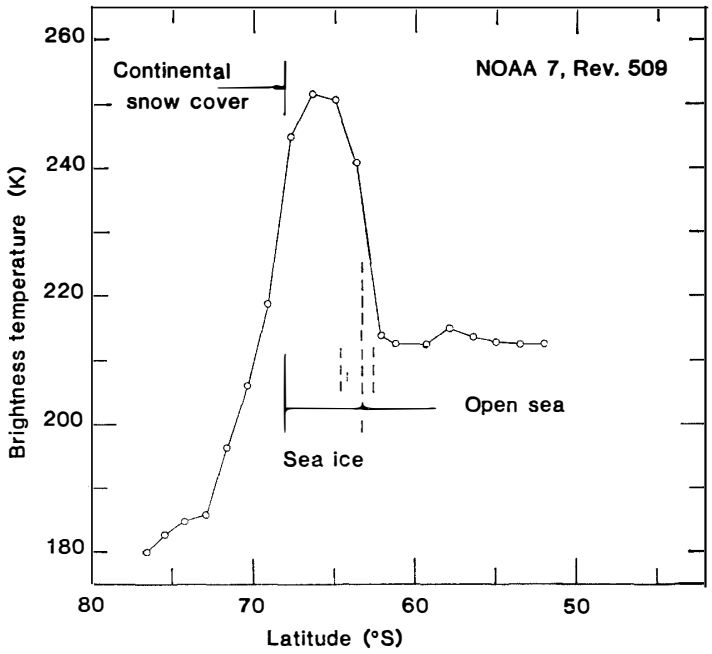

Fig. 5. Distribution of 50.3 GHz brightness temperatures along the nadir points. NOAA-7, revolution 509 on July 27, 1981.

spot at 63.6°S appears to be sea ice. The next two spots at 65.0 and 66.4°S showing 251K are completely covered with sea ice. The emissivity can be roughly estimated from eq. (4). ε for the open sea becomes 0.64, which is a little higher than previously reported, and ε for the sea ice becomes 0.91. If we assume a linear relation between the sea ice concentration in the spot and the brightness temperature (ZWALLY and GLOERSEN, 1977; COMISO and ZWALLY, 1982), the ice concentration at the 63.6°S spot is 74%. However, the present figures have a 30% uncertainty as mentioned in the last section, so they are inadequate to determine the sea ice concentration. For convenience, we define the "sea ice edge" as a spot of 232K ($\pm$10K), which may contain 50% sea ice under a clear calm condition.

The horizontal distribution of 50.3 GHz brightness temperature is shown in Fig. 6, from a single orbit covering the north-eastern part of the Antarctic Ocean. The position of the sea ice edge is described by the solid line by the method explained above. This figure is an example in winter; the ice edge is located about 1000 km from the coast and at about 60°S. Considering the uncertainty of $\pm$10K in the measured brightness temperature, uncertainty in the ice edge is within the two dashed lines. Since the width of these two lines is in the same order as the spot width of the MSU, it will not cause a serious problem in the discussion of present resolution. Data spots at the scan edge are excluded in the analysis, because they may contain much error.

In order to confirm the results, ground truth is required; however, there are no

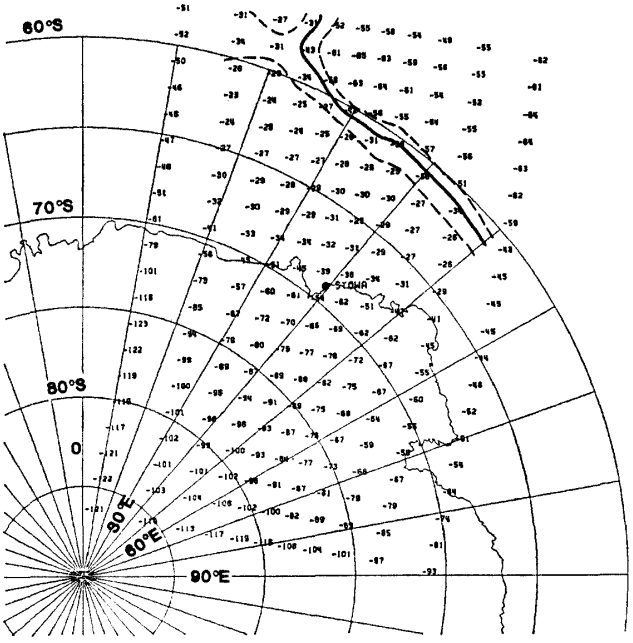

Fig. 6a. Horizontal distribution of 50.3 GHz brightness temperatures (in °C) in winter. The solid line shows the sea ice edge and dashed lines show the deviation of sea ice edge assuming a $\pm$10 K uncertainty in brightness temperature. NOAA-7 revolution 989 on September 1, 1981.

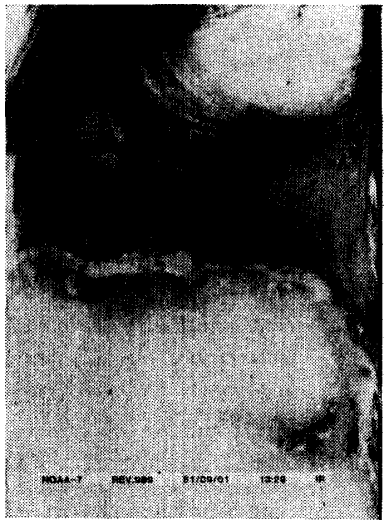

Fig. 6b. Infrared imagery of AVHRR for the same orbit as (a). Geometrical correction is not applied, but the image area roughly corresponds to the analyzed area in (a).

surface data. As a substitute, AVHRR (Advanced Very High Resolution Radiometer) infrared imagery derived from the same orbital data is compared (Fig. 6b). From this figure, the place recognized as the sea ice between the coast of the continent and 60°S where no cloud cover exists is also detected as the sea ice from the microwave data in Fig. 6. However, the region recognized as sea ice from the microwave imagery cannot always be confirmed as sea ice by the infrared imagery, since several regions are covered with clouds. Especially, regions around the ice edge are often covered with clouds and precise confirmation is difficult.

Another example of the horizontal distribution of the 50.3 GHz brightness temperature in summer is shown in Fig. 7a. From this figure, the sea ice edge is determined as the solid line near the coast, about 67°S offshore of Syowa Station. The visible imagery of AVHRR is compared in Fig. 7b. In this figure, a large part of the ice edge is not covered by clouds, and the position of the ice edge determined by the microwave is confirmed by the visible imagery.

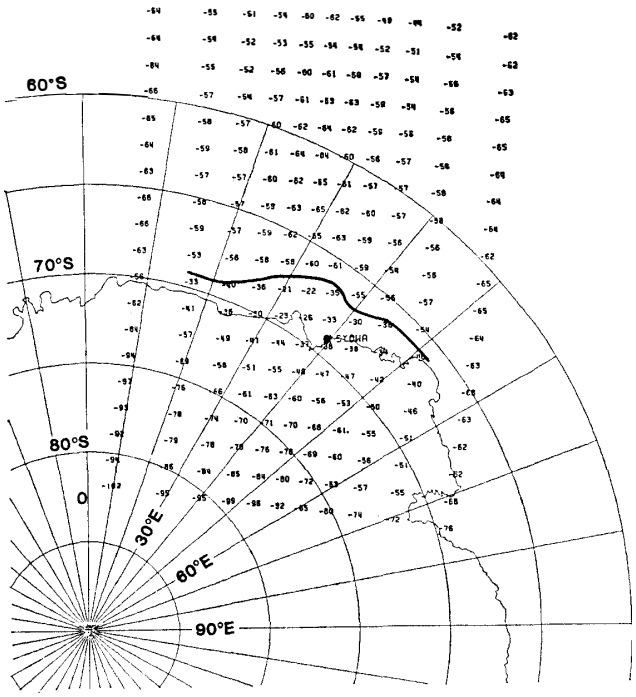

Fig. 7a. Horizontal distribution of 50.3 GHz brightness temperature (in °C) and sea ice edge (solid line) in summer. NOAA-7 revolution 2937 on January 17, 1982.

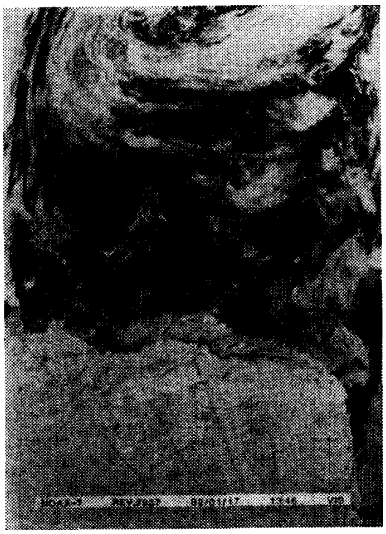

Fig. 7b. Visible imagery of AVHRR for the same orbit as (a).

The seasonal variation of the sea ice edge from February 1981 to January 1982 is shown in Fig. 8 from one set of data per month. The area of the sea ice is a minimum from February to April and increases from May. The maximum sea ice extent is seen in September and October, and in early November in some regions. A rapid retreat of the ice edge occurred during November and January. To the west side of 25°E, the ice edge extends greatly to the north from August to October,

just as seen in the results of Nimbus-5 from 1973 to 1976 (ZWALLY *et al.*, 1983). Recently, COMISO *et al.* (1984) reported sea ice distributions in the Indian Ocean sector from 18 and 37 GHz SMMR data of Nimbus-7 for October and November 1981. Comparing the present result and that from Nimbus, good agreement is found.

Using all of the 50.3 GHz data analyzed, the annual variation of the sea ice edge along 40°E is shown in Fig. 9. Detailed variations can be seen in this figure. The

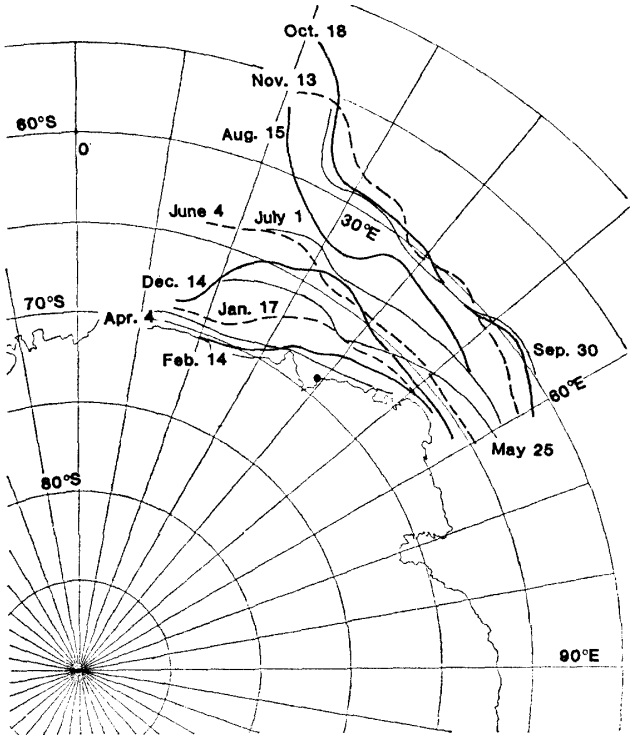

Fig. 8. Variation of sea ice extent during February 1981 and January 1982 derived from 50.3 GHz brightness temperature.

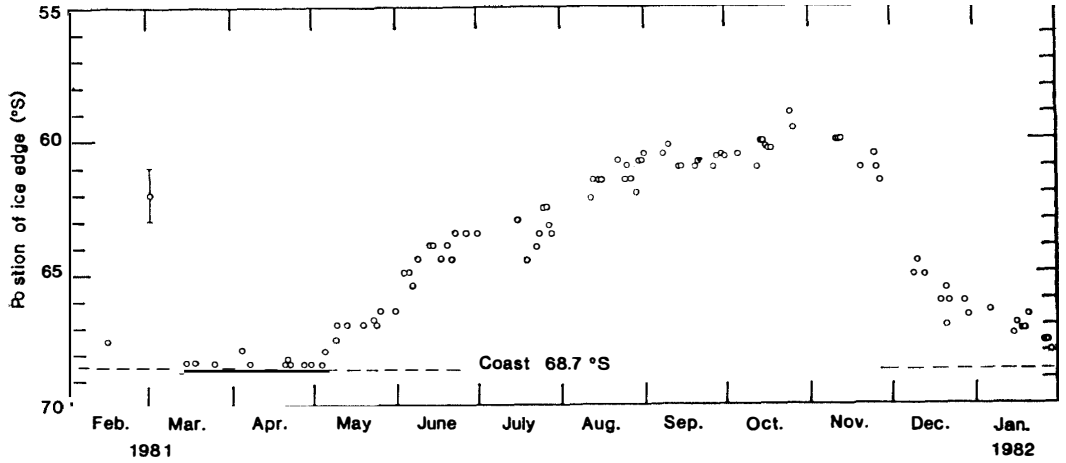

Fig. 9. Positions of ice edge on 40°E meridian from February 1981 to January 1982 obtained from 50.3 GHz brightness temperature.

growth of sea ice starts in the middle of April; in the end of June once the extension stops around 64°S, and from the end of July it starts again till the end of August. During September, October and early November, the ice edge lies at 61–60°S, and at the end of October, the edge shows its maximum extent, to 59°S. The retreat of the ice edge from the end of November to the middle of December is very rapid, at a rate of 2.5° latitude per 10 days, and afterwards very slow. This kind of analysis of the sea ice extent was already done using data from early meteorological satellites such as ITOS and NOAA (KUSUNOKI, 1981); however, the data were visible or infrared imageries and it was difficult to discriminate clouds from sea ice. Irrespective of clear or cloudy weather, the present data have the capability to detect the ice edge automatically. Although the definition of the "ice edge" might be different between the results by the visible or infrared to microwave data, the present result is compared to that of KUSUNOKI (1981). The year 1981 was a year of small extent of sea ice in wintertime, as were 1966, 1967 and 1973.

4. Concluding Remarks

The present method is useful in detecting the sea ice simply, though it has an uncertainty of ± 100km owing to the atmospheric effect and low resolution. It is difficult to derive the sea ice concentration or to classify the age and conditions of sea ice from the MSU data alone. However, if cloud elimination becomes possible from AVHRR imagery and this is combined with the MSU data, a more precise and detailed distribution of sea ice can be obtained. More work on ground truth is needed in the polar regions to confirm the results.

Acknowledgments

The authors wish to express their sincere thanks to the members of JARE-22 led by Prof. Y. YOSHIDA, National Institute of Polar Research, for their kind support in receiving the satellite data. Thanks are also due to Prof. T. YOSHINO of University of Electro-Communications and Profs. S. KAWAGUCHI, K. KUSUNOKI and Mr. M. WADA of National Institute of Polar Research for their kind advice and encouragement throughout this work. The authors are indebted to Miss S. NISHIKAWA for typing the manuscript.

The processing and analysis of the data were done by utilizing facilities of the Information Processing Center of National Institute of Polar Research including the HITAC M-160 II and M-180 systems. This work was supported financially in part by a Grant-in-Aid for Scientific Research, No. 56460038, the Ministry of Education, Science and Culture.

References

COMISO, J. C. (1983): Sea ice effective emissivities from satellite passive microwave and infrared observations. J. Geophys. Res., **88**, 7688–7704.

COMISO, J. C. and ZWALLY, H. J. (1982): Antarctic sea ice concentrations inferred from Nimbus 5 ESMR and Landsat imagery. J. Geophys. Res., **87**, 5836–5844.

COMISO, J. C., ACKLEY, S. F. and GORDON, A. L. (1984): Antarctic sea ice microwave signatures and their correlation with *in situ* ice observations. J. Geophys. Res., **89**, 662–672.

GRODY, N. C. and SHEN, W. C. (1982): Observation of hurricane David (1979) using the Microwave Sounding Unit. NOAA Tech. Rep., NESS, **88**, 52 p.

JAPAN METEOROLOGICAL AGENCY (1982): Meteorological data at the Syowa Station in 1980. Antarct. Meteorol. Data, **21**, 274 p.

KUSUNOKI, K. (1981): Variations of sea ice conditions in Lützow-Holm Bay area, in Antarctica, in the last 20 years. Sea Level Ice and Climatic Change, ed. by I. ALLISON. Wallingford IAHS, 171–176 (IAHS Publ., No. 131).

MAYKUT, G. A. (1978): Energy exchange over young sea ice in the central Arctic. J. Geophys. Res., **83**, 3646–3658.

NORDBERG, W., CONAWAY, J., ROSS, D. B. and WILHEIT, T. (1971): Measurements of microwave emission from a foam-covered, wind-driven sea. J. Atmos. Sci., **28**, 429–435.

SMITH, W. L., WOOLF, H. M., HAYDEN, C. M., WARK, D. Q. and MCMILLIN, L. M. (1979): The TIROS-N Operational Vertical Sounder. Bull. Am. Meteorol. Soc., **60**, 1177–1187.

STEPHENS, G. L. (1978): Radiation profiles in extended water clouds. I: Theory. J. Atmos. Sci., **35**, 2111–2122.

SVENDSEN, E., KLOSTER, K., FARRELLY, B., JOHANNESSEN, O. M., JOHANNESSEN, J. A., CAMPBELL, W. J., GLOERSEN, P., CAVALIERI, D. and MÄTZLER, C. (1983): Norwegian remote sensing experiment; Evaluation of the Nimbus 7 Scanning Multichannel Microwave Radiometer for sea ice research. J. Geophys. Res., **88**, 2781–2791.

TANAKA, S., YOSHINO, T., YAMANOUCHI, T. and KAWAGUCHI, S. (1982): On the satellite remote measurements of vertical temperature profiles of the Antarctic atmosphere. Mem. Natl Inst. Polar Res., Spec. Issue, **24**, 94–100.

WEINREB, M. P., FLEMING, H. E., MCMILLIN, L. M. and NEUENDORFFER, A. C. (1981): Transmittances for the TIROS Operational Vertical Sounder. NOAA Tech. Rep., NESS, **85**, 60 p.

WILHEIT, T. T., Jr. (1978): A review of applications of microwave radiometry to oceanography. Boundary-Layer Meterol., **13**, 277–293.

WILHEIT, T., NORDBERG, W., BLINN, J., CAMPBELL, W. and EDGERTON, A. (1972): Aircraft measurements of microwave emission from Arctic sea ice. Remote Sensing Environm., **2**, 129–139.

ZWALLY, H. J. and GLOERSEN, P. (1977): Passive microwave images of the polar regions and research applications. Polar Rec., **18**, 431–450.

ZWALLY, H. J., COMISO, J. C., PARKINSON, C. L., CAMPBELL, W. J., CARSEY, F. D. and GLOERSEN, P. (1983): Antarctic sea ice, 1973–1976; Satellite passive-microwave observations. NASA Spec. Publ., **459**, 206 p.

(*Received July 17, 1984; Revised manuscript received September 18, 1984*)